Original Research

S. Garré*
T. Günther
J. Diels
J. Vanderborght

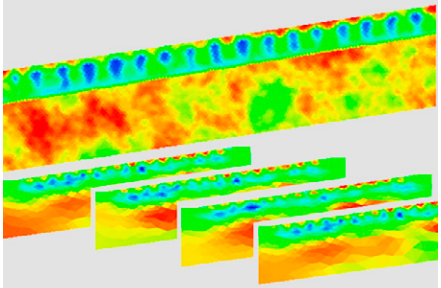

The performance of various ERT arrays to monitor soil moisture dynamics in the field was investigated. Classical measures such as data recovery as well as spatial measures such as semivariances were used for evaluation. The arrays detected distinct patterns under different cropping systems, but variances and semivariances were underestimated.

S. Garré and J. Diels, KU Leuven, Earth and Environmental Sciences, Soil and Water Management, Celestijnenlaan 200E, 3001 Leuven, Belgium. S Garré presently at University of Liège, Gembloux Agro-Bio Tech, Passage des déportés 2, 50 30 Gembloux, Belgium; T. Günther, Leibniz Institute for Applied Geophysics, Stilleweg 2, 30655 Hannover, Germany; J. Vanderborght, Forschungszentrum Juelich GmbH, Agrosphere (IBG-3), 52425 Juelich, Germany. *Corresponding author (sarah.garre@ulg.ac.be).

Vadose Zone J.
doi:10.2136/vzj2011.0186
Received 30 Nov. 2011.
Open Access Article

Evaluating Experimental Design of ERT for Soil Moisture Monitoring in Contour Hedgerow Intercropping Systems

Contour hedgerow intercropping systems have been proposed as an alternative to traditional agricultural practice with a single crop, as they are effective in reducing run-off and soil erosion. However, competition for water and nutrients between crops and associated hedgerows may reduce the overall performance of these systems. To get a more detailed understanding of the competition for water, spatially resolved monitoring of soil water contents in the soil-plant-atmosphere system is necessary. Electrical resistivity tomography (ERT) is potentially a valuable technique to monitor changes in soil moisture in space and time. In this study, the performance of different ERT electrode arrays to detect the soil moisture dynamics in a mono- and an intercropping system was tested. Their performance was analyzed based on a synthetic study using geophysical measures, such as data recovery and resolution, and using spatial statistics of retrieved water content, such as an adjusted coefficient of variation and semivariances. The synthetic ERT measurements detected differences between the cropping systems and retrieved spatial structure of the soil moisture distribution, but the variance and semivariance were underestimated. Sharp water content contrasts between horizons or in the neighborhood of a root water uptake bulb were smoothened. The addition of electrodes deeper in the soil improved the performance, but sometimes only marginally. ERT is therefore a valuable tool for soil moisture monitoring in the field under different cropping systems if an electrode array is used which can resolve the patterns expected to be present in the medium. The use of spatial statistics allowed to not only identify the overall model recovery, but also to quantify the recovery of spatial structures.

Abbreviations: ERT, electrical resistivity tomography.

Agriculture on infertile, shallow or steep soils in the humid tropics often leads to a low efficiency due to a combination of high leaching rates in the growing season and shallow root development of annual food crops (Hairiah et al., 2000). On these soils, erosion and declining soil quality are problematic. Mixed cropping systems are common in traditional production systems in the humid tropics and are an alternative to agricultural practice with a single crop. Contour hedgerow intercropping is a mixed cropping system which involves planting hedgerows of (nitrogen-fixing) plants along the contour lines of a slope at a distance of 4–6 m (Tang, 2000). Hedgerows are usually pruned to reduce shading of crops and to supply biomass for mulching. Contour hedgerow intercropping systems are extremely effective in reducing runoff and controlling erosion on steep slopes (Lal, 1989; Craswell et al., 1997; Morgan, 2004). However, sometimes a negative impact on crop response in the alley has been observed (Agus et al., 1997; Turkelboom et al., 1997; Dercon et al., 2006) due to competition and exposure of infertile soil as a result of tillage on steep slopes. Competition for nutrients and/or water between crops and associated hedgerows may reduce the overall performance of contour hedgerow systems and hampers its acceptance by rural communities (Pansak et al., 2007). To make it a good alternative for traditional monocropping systems, the nature and mechanisms driving this competition need to be understood.

Up until now, mainly the consequences of competition, such as decreased plant productivity and stress symptoms, have been studied (e.g., Hairiah et al., 2000; Imo and Timmer, 2000; Aaltonen and Olofsson, 2002; Dercon et al., 2006; Mushagalusa et al., 2008). To get a more detailed understanding of the competition for water, two-dimensional or three-dimesional monitoring of the water fluxes in the soil-plant-atmosphere system is necessary. As substantial spatial variability is to be expected, point measurements of water content are not sufficient. Geophysical imaging techniques, such as electrical resistivity tomography

(ERT) may solve this problem. Electrical resistivity (ρ) is measured by applying an electrical current through a set of electrodes and reading the resulting differences in electric potential on separate electrodes. Multi-electrode arrays along lines or grids generate measurements of apparent electrical resistivity in multiple soil volumes arranged in two-dimensional or three-dimensional sections (Rossi et al., 2011). A data inversion has to be performed to get the resistivity distribution from the measured apparent resistivities. The result of this inversion is a model which remains a simplified concept of reality fitting the data within error bounds and inversion constraints (Günther, 2004). The measured apparent electrical resistivity depends on soil texture and structure (e.g., Besson et al., 2004), stone content (Cousin et al., 2009), soil moisture content and soil water salinity (Archie, 1942; Waxman and Smits, 1968; Revil and Glover, 1998; Linde et al., 2006???; Laloy et al., 2011), temperature, and in some cases on root biomass (Amato et al., 2008; Zenone et al., 2008; Amato et al., 2009; al Hagrey and Petersen, 2011). Changes of these variables with time, such as soil moisture changes, can thus be followed performing resistivity measurements at several times provided a good calibration relationship between electrical resistivity and the variable under consideration.

ERT has been used before to observe transient state phenomena in the soil-plant continuum by several authors. On the one hand, many publications deal with the water uptake of trees: olive and apricot tree (al Hagrey, 2007; Celano et al., 2010; Celano et al., 2011), poplar tree (al Hagrey, 2007) and natural forest (Nijland et al., 2010). On the other hand, ERT has also been used to monitor water use of agricultural crops (Michot et al., 2001; Michot et al., 2003; Werban et al., 2008; Amato et al., 2009; Srayeddin and Doussan, 2009; Garré et al., 2011). The majority of performed studies stress the promising capabilities of the ERT-technique, but the difficulties to interpret the measured electrical resistivity remain, certainly under field conditions. First, as the resistivity is affected by several factors, the variability of these factors needs to be restricted or measured independently and a fitting calibration equation needs to be established (Michot et al., 2003; Celano et al., 2011; Garré et al., 2011). Second, possibly rapid changes in the plant-soil continuum, such as a passing infiltration front after heavy rain or a tracer pulse, require high temporal resolution of the measurement to avoid temporal smearing (e.g., Koestel et al., 2009). Finally, root water uptake processes are spatially variable, small-scale processes, which require at least decimeter resolution and sensitivity to approximately a 10% moisture change to be able to monitor changes in time and space (Michot et al., 2003; Srayeddin and Doussan, 2009).

Many of the above-mentioned issues might be tackled using an appropriate electrode alignment and measurement configuration. The optimal ERT survey should be designed to meet the objectives of the experiment (Stummer et al., 2004), as different set-ups represent different distribution and amount of data information, signal-to-noise levels and time resolution. If time would not be an issue, one could measure any total comprehensive data set. Noel and Xu (1991) defined this as "a suite of non-reciprocal electrode configurations comprising all subsurface information an n-electrode array is capable of gathering." However, this data set quickly contains several thousands of measurements for only a few electrodes (see Xu and Noel, 1993), which is generally unfeasible. Therefore, the information contained in other, smaller classical measurement arrays has been explored using various measures (Spies, 1989; Curtis, 1999; Alumbaugh and Newman, 2000; Maurer et al., 2001; Friedel, 2003; Furman et al., 2003; Stummer et al., 2004; Oldenborger and Routh, 2009). To calculate these measures, an assumption about the subsurface to be measured has to be made beforehand. The information content of a 'non-comprehensive' survey does not only depend on the type of survey, but also on the medium to be measured, or more specifically, on its statistical resistivity distribution. Recently, Blome et al. (2011) developed a method to maximize the information content from a pole-dipole data set without having to make assumptions about the subsurface resistivity distribution. All papers mentioned above considered arrays with only surface electrodes. However, inclusion of subsurface electrodes in ERT measurement arrays may be simple way to obtain measurement configurations with a higher information content. The above-mentioned studies focus on the one-to-one data recovery after inversion. However, this is often a too stringent criterion to evaluate the performance of a measurement. It focuses on a cell to cell data recovery, whereas in many applications one of the most important issues is the recovery of spatial structures and their changes in time. Singha and Gorelick (2005) monitored the movement of a tracer plume with ERT and evaluated the quality of the measurements using mass recovery and an analysis of the center of mass and spatial variance of the imaged tracer plume. Also in the domain of solute transport in the soil, the use of solute transport parameters from breakthrough curves and spatial correlation in resistivity images was used as an alternative quality analysis (Kemna et al., 2002; Vanderborght et al., 2005; Müller et al., 2010). These studies point out that for the evaluation of ERT for application in the field of soil hydrology we should widen our outlook and use measures which tell us more about the capabilities of ERT to observe the processes we are interested in.

The main aim of this paper is to demonstrate a methodology for preparing ERT measurements of soil water dynamics for the specific case of a sloping field under tropical climate conditions with monocropping and intercropping systems. More specifically, the objectives are to (i) generate realistic soil moisture distributions and resulting resistivity as can be expected under a monocropping and intercropping systems, (ii) analyze the performance of different measurement arrays using spatial statistics of recovered soil moisture contents and classical geophysical measures like e.g., recovery, coverage and resolution radius, and (iii) identify an optimal survey design to capture the generated patterns with ERT during a growing season.

Concerning the electrode arrays, we will consider surface electrode arrays and evaluate the additional value of including buried electrodes in these arrays. We will use classical and well tested measurement configurations. To evaluate the performance of the ERT inversion, we will use methods such as data recovery, sensitivity and resolution radius, but include also other means of quantification such as an adjusted coefficient of determination and a semivariogram and evaluate their performance as inversion quality indicators. To perform these analyses, we will work with a synthetic dataset.

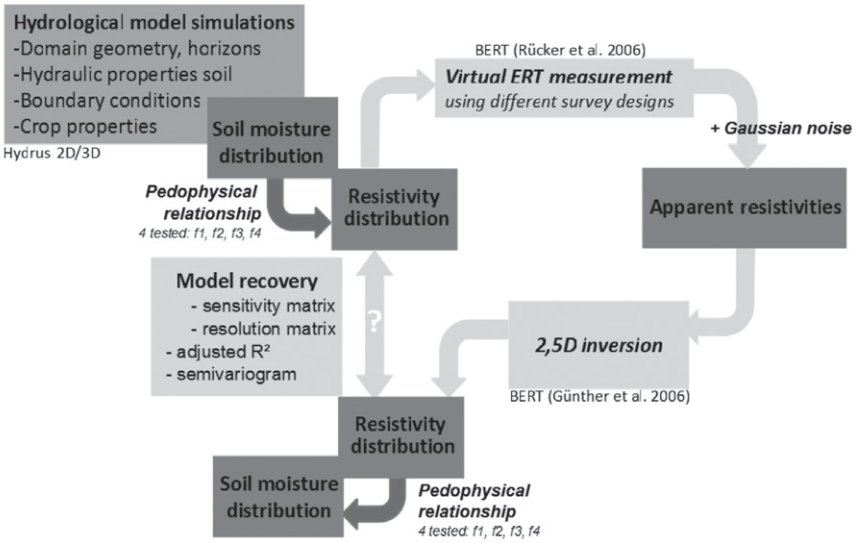

Fig. 1. Overview of the approach followed to identify the optimal ERT survey design for studying soil water dynamics under different two different cropping systems

Material and Methods

General Approach

Figure 1 shows the approach followed in this paper to identify the optimal ERT survey design for studying water fluxes under two different agricultural systems. First, a hydrological model is created approaching the soil, relief and climate conditions at a field site near Suan Phung, Ratchaburi Province, Thailand (see the Hyrdological Model section). Two cases are simulated: a field plot with only maize and one with contour hedgerow intercropping with *Leucaena leucocephala* L. After a spin-up period of 30 d, the model was run for 130 d starting from maize sowing. Second, a pedo-physical relationship was used to convert the water content distribution of a few characteristic timeframes to a resistivity distribution (see the From Water Content to Resistivity section). We used four pedo-physical relationships of which one was a fit to measurements conducted in a calibration pit in the field site near Suan Phung. The other three equations were used to assess the effect of using a deviating relationship on the assessment of the optimal survey design. Third, virtual ERT measurements were conducted by forward modeling using different measurement configurations and the simulated two-dimensional distribution of resistivities (seethe Experimental Design section). We added noise to the simulated measurements equal to 1% of the resistivity value to approach real measurements which are always prone to background and measurement noise. After that, the data were inverted using a regularization strength such that data were fitted within the noise level, and the resolution and sensitivity matrix were analyzed (see the Inversion and Measures for Survey Performance section). Finally, we compared the original resistivity distributions with the inverted ones to obtain the model recovery (see the Inversion and Measures for Survey Performance section). Measures for spatial variability as well as the resolution matrix, sensitivity matrix (based on the recovered resistivity maps) and model recovery (based on recovered water contents) were then used to judge the performance of the measurement arrays.

Hydrological Model

The hydrological model was set up using a modified version of Hydrus2D/3D (Šimůnek et al., 1996), which allows modeling of root water uptake by two different crops simultaneously. The simulations were run on a soil cross-section of 13-m length and −3-m depth with an inclination of 15%, i.e., like experimental plots at a field site near Suan Phung, Ratchaburi province, Thailand. Two cases were simulated: maize (*Zea mays* L.) monocropping and contour hedgerow intercropping with rows of *Leucaena leucocephala*, maize, and bare soil strips accounting for a few chili plants with low soil coverage. We assume that we can ignore the heterogeneity of the third dimension, since the biggest contrasts occur because of the root water uptake in the simulation and because of the transition between horizons. Since the plants are planted row-wise along the third dimension, we do not expect that the heterogeneity will change much in the third dimension. Also the horizon boundaries can be assumed to be continuous in the third dimension. As such, we neglect the effect of soil heterogeneity in the third dimension.

Figure 2 gives an overview of the model. The soil consist of three horizons: A_p, B and C. A_p represents a small disturbed layer from limited tillage (loam), B is an undisturbed soil horizon (sandy-clay-loam) and C represents strongly weathered rock material, a horizon which is difficult to penetrate for roots, but has quite some porosity (clay loam). The hydraulic parameters of these soil horizons are given in Table 1. These soil hydraulic parameters are just a rough approximation of the soil hydraulic properties, estimated from the textural characteristics of samples of the field site using the class pedotransfer function of Carsel and Parrish (1988). For detailed predictive hydraulic modeling of the field site, hydraulic characteristics should be obtained by inverse modeling using long term field data. It was assumed that the perennial Leucaena was capable of developing roots in the C horizon, but that maize did not. The maize plants had a maximal rooting depth of 1 m, whereas the rooting depth of Leucaena was 1.5–2 m. Distance between

maize rows was 0.75 m and between the Leucaena hedges 6 m (see also Fig. 2).

We adopted the Feddes root water uptake model with P0 = −10 cm, Popt = −25 cm, P2H = −500 cm, P2L = −500 cm, P3 = −8000 cm, r2H = 0.5 cm d^{-1} and r2L = 0.1 cm d^{-1} for both crops. See Feddes et al. (1978) and the Hydrus manual (Šimůnek et al., 1996) for more information on these parameters. The hydraulic properties were represented by the van Genuchten equation (van Genuchten, 1980). We accounted for spatial variability in soil hydraulic properties by applying a scaling factor (y) on the hydraulic conductivity and the pressure head (Miller-Miller similitude) of all three horizons, assuming log10(y) has a standard deviation of 0.434 and a correlation length of 1 m in both directions. Scaling factors are used in soil physics to relate the hydraulic properties at a given location to the mean properties at an arbitrary reference point. Rainfall and potential reference evapotranspiration were taken from an on-site weather station for the growing season of 2009. The reference evapotranspiration for a grass reference surface was calculated for hourly time intervals using the Penman–Monteith equation from hourly measurements of solar radiation, wind speed, vapor pressure, end air temperature (Allen et al., 1998). Based on these climatological data, potential evapotranspiration rates for maize (ET_M) and Leucaena (ET_L) and the potential evaporation rate (E_B) for bare soil were calculated using the Aquacrop model (Raes et al., 2009; Steduto et al., 2009) (see Fig. 3). After a spin-up period of 30 d, maize was virtually sown and the Hydrus 2D/3D model was run for 130 d. The initial condition was set using a uniform pressure head of −500 cm. Three timeframes at t = 0, 60, and 108 d yielded characteristic and distinct soil moisture distributions, which were used as input for the experimental design of the ERT survey. The first timeframe represents the soil at the beginning of the growing season. The top soil is dry and the distribution of soil moisture is rather homogeneous in the different soil horizons. The second timeframe at t = 60 d represents the soil in the middle of the growing season. Crops are taking up water and sporadic rainfall wets the soil. The last timeframe at t = 108 d represents the beginning of the strong rainfall period in which the soil is replenished and infiltration fronts become visible in the soil.

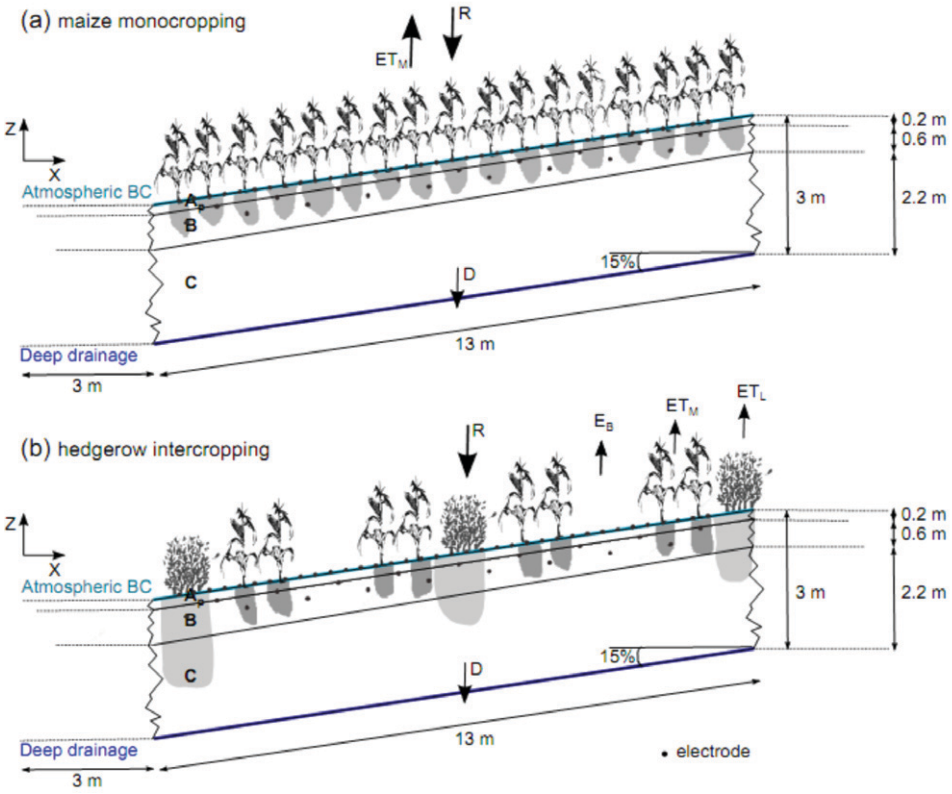

Fig. 2. Hydrological model set-up with top and bottom boundary conditions (BC) for a field plot with (a) only maize and (b) with contour hedgerow intercropping with Leucaena, maize and bare soil strips. Three soil horizons are indicated on the scheme: A_p (0–0.2 m), B (0.2–0.8 m),C (0.8–3 m). Symbols: ET_M: evapotranspiration of maize rows, ET_L: evapotranspiration of leucena strips, E_B: evaporation from bare soil strip, R: rainfall, D: drainage.

Table 1. Soil hydraulic parameters of the van Genuchten–Mualem equation used in the hydrological model.

	θ_r	θ_s	α	n	K_s	l
			cm^{-1}		cm d^{-1}	
A_p	0.078	0.43	0.036	1.56	24.96	0.5
B	0.100	0.39	0.059	1.48	31.44	0.5
C	0.095	0.41	0.019	1.31	6.24	0.5

From Water Content to Resistivity

The water content of the selected timeframes was converted to an electrical conductivity (EC) distribution using one single pedo-physical relationship for all horizons. This pedo-physical relationship was a fit of EC–WC data in a calibration pit in the field to the simplified Waxman and Smits model (Waxman and Smits, 1968):

$$EC_b = \frac{1}{\varphi} WC^n + EC_s \quad [1]$$

where EC_b (S m^{-1}) is the bulk electrical conductivity ($\rho_b = 1/EC_b$), φ (Ω.m), n, and EC_s (S m^{-1}) are fitting parameters. The water content data were obtained using a TDR probe and the EC data were obtained using four electrodes in Wenner configuration (10-cm spacing). The electrodes, the TDR probe and a temperature sensor for temperature correction were installed in the vertical wall of a calibration pit at z = −0.25 m. However, as often there is no information yet on the pedo-physical model at the planning phase of an experiment, we also assessed the quality of the ERT inversion for different pedo-phyiscal models. The parameters of the measured and the three relationships deviating from the measured one are given in Table 2 and Fig. 4 shows the relationship together with functions from literature. It must be noted that we neglect the potential effect of changing root biomass on the pedo-physical relationship in cropped systems. Since the effect is not univocal in the literature, it is impossible to incorporate it without specific experimental data. The effect of the pedo-physical function (f1, f2, f3, and f4) was only assessed using timeframe t = 60 d. For t = 0 and t = 108 d, only the measured function (f4) was applied.

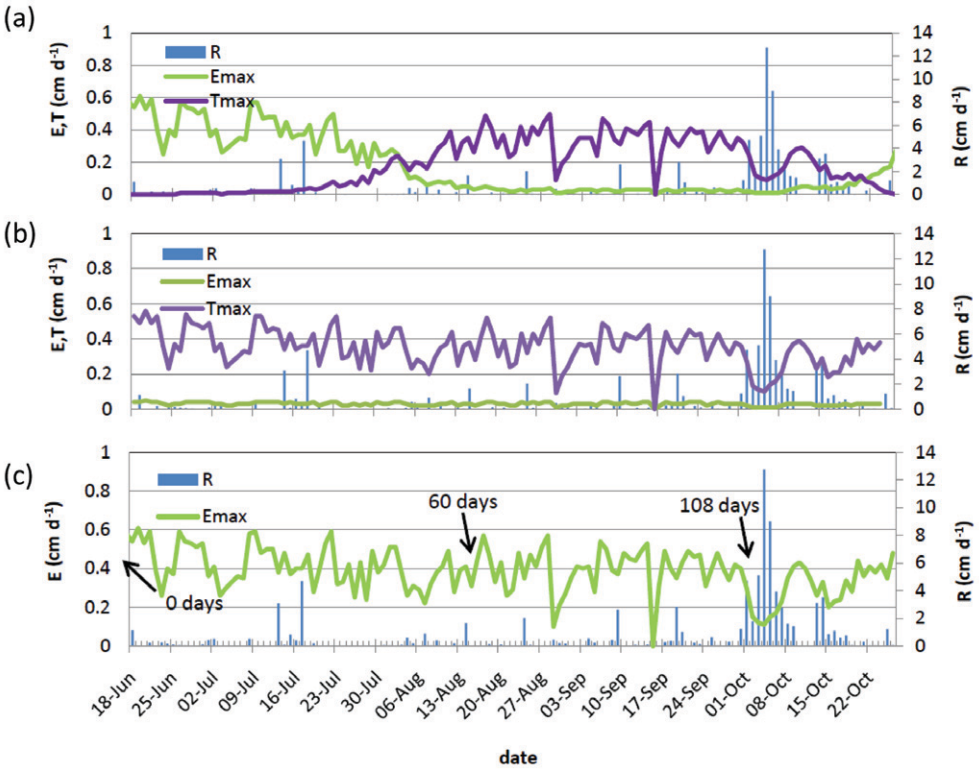

Fig. 3. Rainfall (R), potential evaporation (Emax) and potential transpiration (Tmax) for (a) maize, (b) leuceana and (c) bare soil.

Table 2. Parameters of the simplified Waxman and Smits (1968) model for the four pedo-physical relationships used to convert the simulated water content distribution to a resistivity distribution.

-	ϕ	n	EC_s
-	Ωm	–	S m^{-1}
f1	14.000	1.500	3.0×10^{-3}
f2	10.000	1.100	3.0×10^{-3}
f3	12.000	1.600	2.5×10^{-4}
f4 (measured)	7.237	1.658	5.0×10^{-6}

Experimental Design: ERT Electrode Arrays Under Consideration

The main water fluxes in the soil on a steep slope with crop rows following the contour lines are expected to be vertical, due to evapotranspiration, and along the slope, due to subsurface flow (Harr, 1977; Hornberger et al., 1991; Gutiérrez-Jurado et al., 2006; Essig et al., 2009). A plane of surface and subsurface electrodes along the slope, generating a two-dimensional image of the subsurface along the slope, reduces the modeling effort considerably and is an acceptable way to capture the resulting soil moisture distributions. The main contrasts in water content result from root water uptake and horizon transitions. Since the crops are sown in rows and the horizons are continuous, the heterogeneity in the third dimension is much smaller than in the two-dimesional plane. It must be noted that some of the fine-scale effects of three-dimensional heterogeneity will get lost using this approach. As the resolution should be in the decimeter range to measure root water uptake, the electrode separation should be in this range as well. On the soil surface, 36 electrodes are placed 0.33 m apart. At −0.25 and −0.50-m depth, nine electrodes were placed at each depth level with a horizontal separation of 1.32 m. Four classical measurement configurations were selected based on their distinct sensitivity distributions (Loke and Barker, 1996): the Wenner-array, the dipole-dipole array, the pole-dipole array and a combination of the dipole-dipole and the Wenner array. For each array, we considered data sets using only surface electrodes and datasets including also subsurface electrodes to assess the increase in data information due to deeper electrodes. The electrode configurations with deeper electrodes have no measurements crossing the different depth levels. They are used as a second and third line in which the same array type is exerted as for the surface electrodes. The additional measurements stay confined to the depth levels.

Inversion and Measures for Survey Performance: "Classical" Measures of Survey Performance (Resolution Matrix, Data Coverage, Model Recovery)

For the inversion, we minimize the following objective function (Φ) composed of a data functional (Φ_d), a regularization parameter (λ) and a model functional (Φ_m) (Günther et al., 2006):

$$\Phi = \Phi_d + \lambda \Phi_m \rightarrow \min \quad [2]$$

in which

$$\Phi_d(\mathbf{m}) = \mathbf{D}\left\|(\mathbf{d} - \mathbf{f}(\mathbf{m}))\right\|_2^2 \quad [3]$$

and

$$\Phi_m(\mathbf{m}) = \left\|\mathbf{C}(\mathbf{m} - \mathbf{m}^0)\right\|_2^2 \quad [4]$$

where **m** is the model vector, **d** the data vector, **f(m)** the forward response of the model, $\mathbf{m}^0$ is a starting or reference model. **D** is the data weighting matrix, i.e., a diagonal matrix with inverse errors on the main diagonal, and **C** the model smoothness matrix. Note that we are using logarithmized quantities, i.e., $\mathbf{m}_i = \log(\rho)$ and $\mathbf{d}_i = \log(\rho_a)$. As explained in Rücker et al. (2006), we impose Neumann conditions at the soil surface to avoid current flow through the boundary. The other boundaries are treated with mixed boundary conditions after Dey and Morrison (1979). The formulation of boundary conditions for the solution of the partial differential equations requires boundaries at the modeling domain that are generally far from the sources and parameter contrasts. The individual time-steps were processed independently, since we are not analyzing a time series here. Between the three time steps there was a gap of 60 and 48 d. It must be noted that a timelapse scheme regularizing the differences to the first or preceding timestep should further improve inversion results and should be used when handling a time series. The independent inversion can be seen as the lower limit of what is possible.

Several measures can be used to assess the quality of the information obtained by inversion of the measurements produced by a certain electrode array. A first measure is the *distribution of the cumulative sensitivity or coverage* (S_{cum}) (e.g., Furman et al., 2003; Günther, 2004), which is for a model cell (j) the sum of the absolute sensitivity values ($S_{i,j}$) of all N data points (i):

$$S_{cum,j} = \sum_{i=1}^{N} \left| S_{i,j} \right| \quad \text{with } S_{i,j}(\mathbf{m}) = \frac{\partial f_i(\mathbf{m})}{\partial m_j} \quad [5]$$

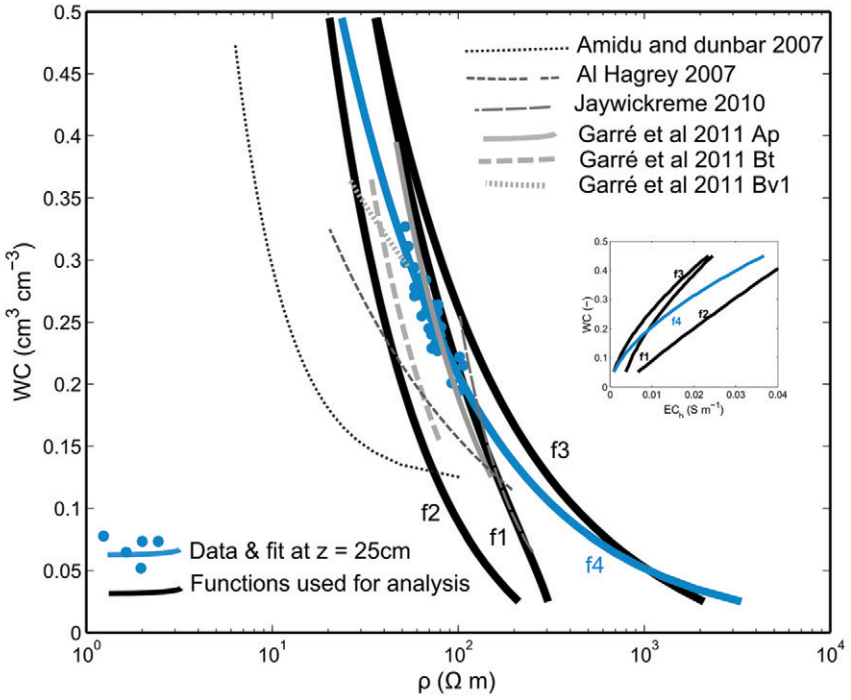

Fig. 4. Pedo-physical functions plotted with other pedo-physical functions from literature (al Hagrey, 2007; Amidu and Dunbar, 2007; Jayawickreme et al., 2010; Garré et al., 2011).

S_{cum} indicates how the individual model cells are covered by the measurements. To compare this cumulative sensitivity between different electrode arrays, it has to be normalized by the number of data points (N) and the mesh cell size (A_{cell_j}). Mesh cells with a log10(coverage) < 0.8 were excluded from further analysis.

A second measure is the *resolution radius* (r) of a model cell. We first calculated the diagonal elements of the resolution matrix **R**. They are a quantitative measure of the independence of the inverted values (Menke, 1989). A diagonal element $R_{jj} = 1$ indicates perfect resolution of the resistivity in the model cell j, whereas $R_{jj} = 0$ proves that this cell is completely unresolved (Günther, 2004; Stummer et al., 2004). The resolution matrix (**R**) of a nonlinear problem can be retrieved by solving:

$$\mathbf{R} = (\mathbf{S}^T\mathbf{D}^T\mathbf{D}\mathbf{S} + \lambda\mathbf{C}^T\mathbf{C})^{-1}\mathbf{S}^T\mathbf{D}^T\mathbf{D}\mathbf{S} \quad [6]$$

Friedel (2003) indicated that a resolution radius can be determined for each model cell. The concept of the resolution radius allows comparing the resolution of inversions using e.g., different mesh cell sizes. r_j is the radius of a sphere at the midpoint of the jth cell having a resolution of 1, assuming a piecewise constant cell resolution. For a triangular mesh with A_{cell_j} the area of the jth model cell, the resolution radius is:

$$r_j = \sqrt{\frac{A_{cell\_j}}{R_{jj}/\pi}} \quad [7]$$

A third measure is the *model recovery*, which is the difference between the model input and the result after inversion for each model cell, normalized by the input resistivities or the mean resistivity of the model (not shown). This measure is affected by the data information of the array, as well as by the errors made during the inversion process. Model recovery can be calculated for the all mesh cells or for average behavior, such as a one-dimensional profile. We calculated a root mean squared error (RMSE) for the inverted and modeled one-dimensional water content profiles. In addition to the model recovery after an inversion with perfect knowledge of electrode placement, we also tested the effect of inaccurate electrode placement on the model recovery for the intercropping case at $t = 60$ d for all arrays with deeper electrodes. In some cases, this effect can be important to acknowledge (Wilkinson et al., 2008; Danielsen and Dahlin, 2010). For the four classical measurement configurations with deep electrodes at $t = 60$ d, we shifted each electrode at random in the x or z direction using a normally distributed pseudorandom number distribution with standard deviation 0.03 m in the input file for the inversion.

Measures for Spatial Variability

Cell-to-cell comparison of model recovery is a very stringent criterion for model performance in which a few local mismatches might affect the evaluation to a major extent. In hydrological studies, the main interest is often to capture the spatial patterns which are present in the soil moisture distribution. To test the performance of the different arrays to capture this spatial variability, we defined two criteria: an adjusted coefficient of determination (Theil, 1971; p. 164, p. 175–178) and the spatial correlation using a semivariogram for each of the tested arrays.

The adjusted coefficient of determination (R_{adj}^2) indicates which fraction of the spatial variability of the simulated WC is explained by the WC derived from ERT measurements and is defined as:

$$R_{adj}^2 = 1 - \frac{\sum_{i,z}\left\{\left[\left(WC_{inv,i,z} - \langle WC_{inv}\rangle_z\right) - \left(WC_{mod,i,z} - \langle WC_{mod}\rangle_z\right)\right]^2\right\}}{\sum_{i,z}\left\{\left[\left(WC_{mod,i,z} - \langle WC_{mod}\rangle_z\right)\right]^2\right\}} \quad [8]$$

in which $WC_{inv,i,z}/WC_{mod,i,z}$ is the inverted/simulated water content for mesh cell i in depth class z (0–0.1 m, 0.1–0.2 m, ..., 2.9–3 m) and $<WC_{inv}>_z$ is the average water content of the inverted mesh for depth class z and this for a selected timeframe. This measure is different from a one-to-one comparison since it corrects one-to-one differences for possible biases in the estimate of the mean water content at a certain depth. As a consequence, this criterion indicates how well the spatial variability is reconstructed but not how well the mean WC at a certain depth is reconstructed. The R_{adj}^2 is used in this paper to judge the recovery of the spatial patterns of soil moisture after inversion.

Similar information as from the adjusted R_{adj}^2 can be retrieved from a crossplot of simulated versus inverted standard deviations of the WC at a certain depth. A clustering of the deviations from the mean around the 1:1 line indicates that not only the total variability but also the patterns of the soil moisture variability are represented well by ERT. A perfect inversion would result in a 1:1 line and a R_{adj}^2 of 1. R_{adj}^2 might be negative in some cases.

We also compared the spatial structure of ERT-derived water contents and model-derived water contents by comparing their semivariograms. The semivariances show the average degree of dissimilarity between two nearby values for a given distance between these values (Deutsch and Journel, 1997). The semivariance is defined as half of the average squared difference between two attribute values separated by vector **h**:

$$\gamma(\mathbf{h}) = \frac{1}{2N(\mathbf{h})}\sum_{i=1}^{N(\mathbf{h})}(x_i - y_i)^2 \quad [9]$$

where $N(\mathbf{h})$ is the number of pairs, **h** is the separation vector, x_i is the value at the start of the pair i, and y_i is the corresponding end value. The semivariogram gives information about the nature and structure of spatial dependency in a random field. At a certain distance the semivariogram levels out. The distance where the model first flattens out is known as the range. The value at which the semivariogram model attains the range is the sill. Observations spatially separated by more than the range are uncorrelated. A semivariogram waving around the sill points to periodicity in the data set, which can be expected working in an agricultural context with crops planted in rows with a fixed inter-row distance. As such, the semivariogram provides additional information on spatial variability and patterns of modeled and inverted data sets.

Results

Resistivity Distributions

Figure 5 shows the modeled resistivity derived from the Hydrus2D simulations and the pedo-physical model f4 together with the inverted resistivities derived from different ERT measurement arrays for the three distinct timeframes ($t = 0$, 60, and 108 d after sowing of the maize) and the monocropping system. This image shows the different patterns present in the simulations and illustrates that the spatial variability of soil moisture is highest in the A and B horizon.

At $t = 0$ d, inverted resistivities match the pattern up to approximately −1 m well, but deeper down the small scale soil heterogeneity seems not to be captured. The patterns are 'lumped' into larger regions with a corresponding 'average' resistivity for that area. The Wenner array seems to fade out patterns in the deepest layer more than the other arrays. At $t = 60$ d root water uptake bulbs are detected by the ERT measurement, but smoothed. Even though the water content didn't change much in the C horizon,

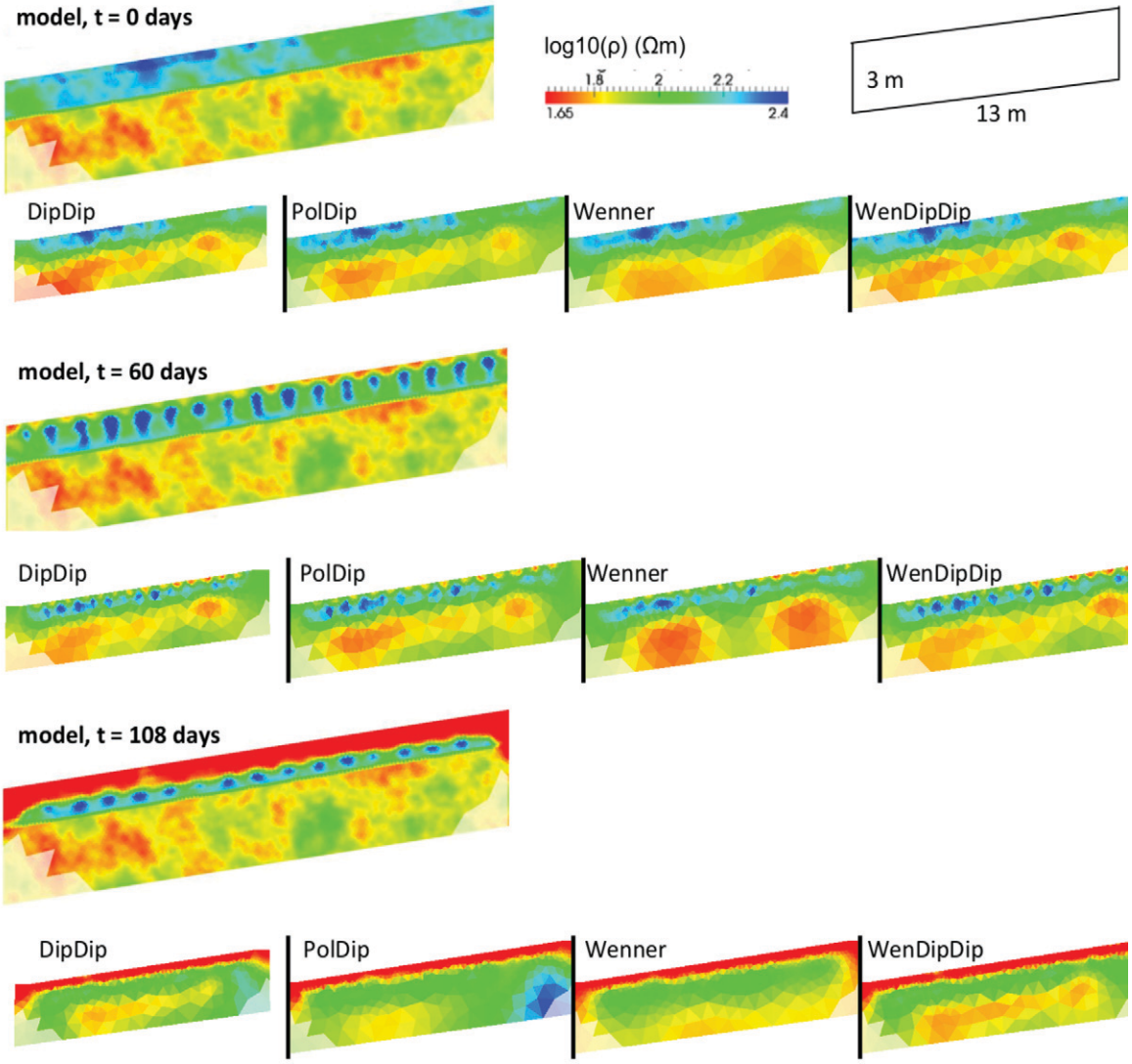

Fig. 5. Model and inverted resistivity (ρ in Ωm, logarithmic scale) at t = 0, 60, and 108 d for the simulations with monocropping (pedo-physical function f4).

the Wenner array gives a different spatial distribution of resistivities than for t = 0 d. At t = 108 d, the low resistivity front at the surface caused by rain water infiltration seems to affect the inversion performance deeper down to a large extent.

Figure 6 shows the difference between the mono- and intercropping system at t = 60 d for modeled and inverted resisitivities. The intercropping system differs from the monocropping system by the deeper and more extensive root water uptake by the Leucaena hedge and the increased drying of the soil.

One-Dimensional Water Content Recovery

A first aspect to be tested was the ability of the different arrays to measure a correct one-dimensional averaged water content profile. Figure 7 shows the one-dimensional water content (WC) profiles for the mono- and intercropping case at t = 0, 60, and 108 d for a profile of 2-m width and 3-m depth in the middle of the simulated domain. In general, ERT predicts the one-dimensional profiles well. However, in the areas of sudden resistivity contrasts, the inverted water content profiles look smoothened and do not follow the jumps. The largest deviations between the one-dimensional WC profile of the model and the one-dimensional WC profile of the inversion are found at t = 108 d, with absolute RMSE between 0.025 and 0.0338 Ωm. Over all timesteps, the Wenner array with only surface electrodes gives the poorest results (0.0272 Ωm < RMSE < 0.0358 Ωm) and the WenDipDip array with deep electrodes included gives the best results (0.0163 Ωm < RMSE < 0.03 Ωm). The largest difference in performance between the various arrays occurs at t = 60 d. Here, the standard deviation of the RMSE is 0.007 Ωm and 0.006 Ωm for the mono- and intercropping case, respectively. ERT is however capable of detecting

differences between the mono- and the intercropping case. The A and B horizons become dryer in the intercropping system at t = 60 d, which is clearly visible in the one-dimensional profiles. The different arrays give way to similar one-dimensional profiles, whereas in most cases, the combination of dipole-dipole and Wenner and the pure dipole-dipole measurements are closest to the model curve. As for the one-dimensional profiles, there is no systematic difference between the arrays with deeper electrodes (All) and those with only surface electrodes (OS), although below −2 m, many of the OS arrays end up further from the model profile than the All arrays and have a the comparison of their one-dimensional WC profiles results in a higher RMSE.

Spatial Variability of Water Content

In addition to a recovery of mean WC values (see one-dimensional water content recovery), it is important to have a good estimate of spatial variability of soil moisture. The recovery of the spatial variability in the mono- and intercropping case and for t = 60 d is shown in Fig. 8. The standard deviation of the water content distribution in the model is plotted against the standard deviation of the WC distribution of the inversion. This is done for depth classes of 0.10 m, so each circle/square represents the value for a specific depth class (color scale) at t = 60 d. The closer the points are to the 1:1 line, the better the inversion reproduces the spatial variability of the model. Generally, the spatial variability of the inversion results is lower than the one of the synthetic model. All arrays capture the high variability between 0 and −1 m and a decreased variability beneath −2 m. The Wenner array underestimates the variability the most, also near the soil surface. For z < −1.75 m, the standard deviation is underestimated by almost all arrays. When the electrode coordinates given for the inversion

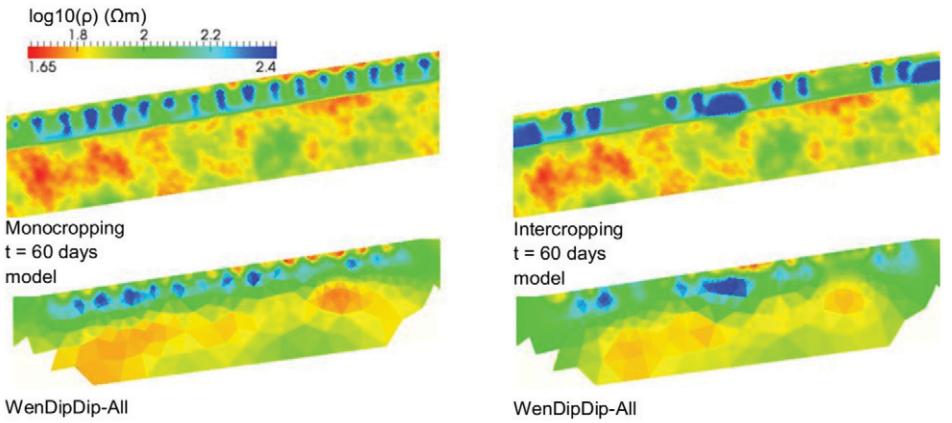

Fig. 6. Modeled and inverted resistivity (ρ in Ωm, logarithmic scale) at t = 60 d for monocropping and intercropping (pedo-physical function f4).

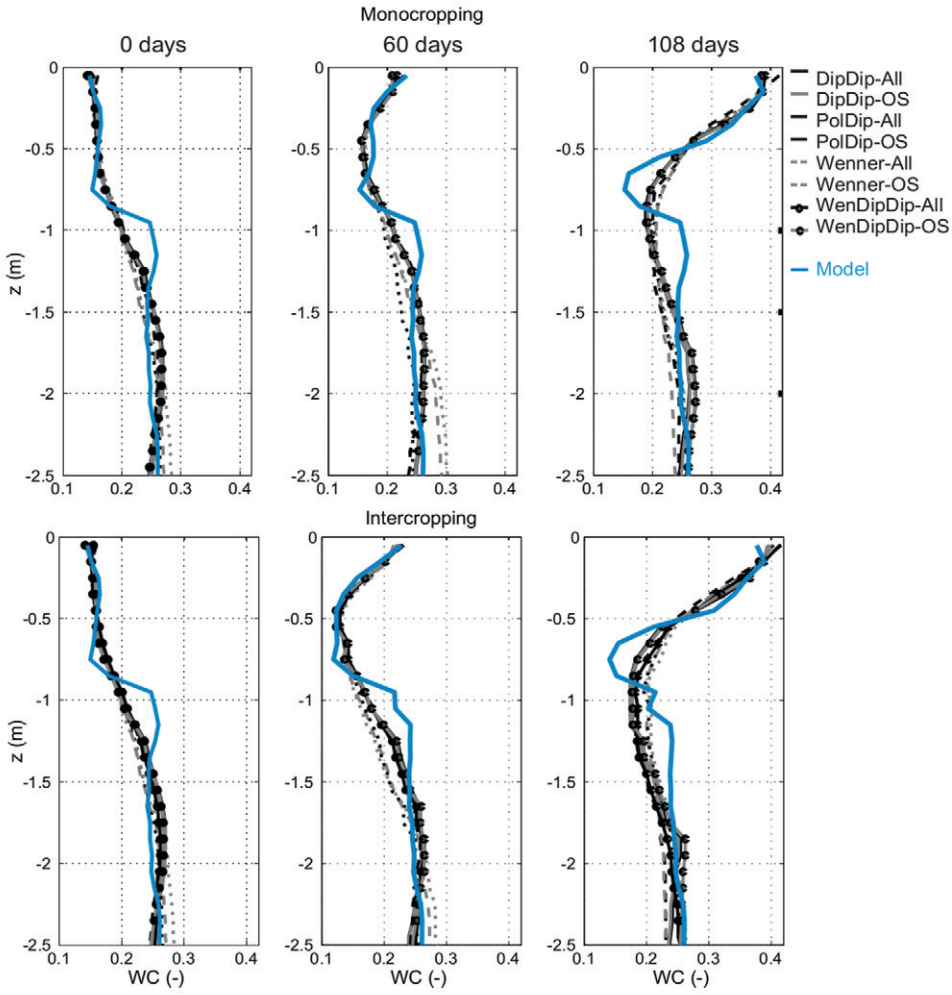

Fig. 7. One-dimensional water content profiles for the mono- and intercropping case at t = 0, 60, and 108 d for a profile of 2-m width and 3-m depth in the middle of the simulated domain. The simulated values are represented by the thick, blue line. DipDip = dipole-dipole, PolDip = pole-dipole, WenDipDip = combination of Wenner & Dipole-dipole. Electrode arrays using only surface electrodes are marked by surface electrodes (OS).

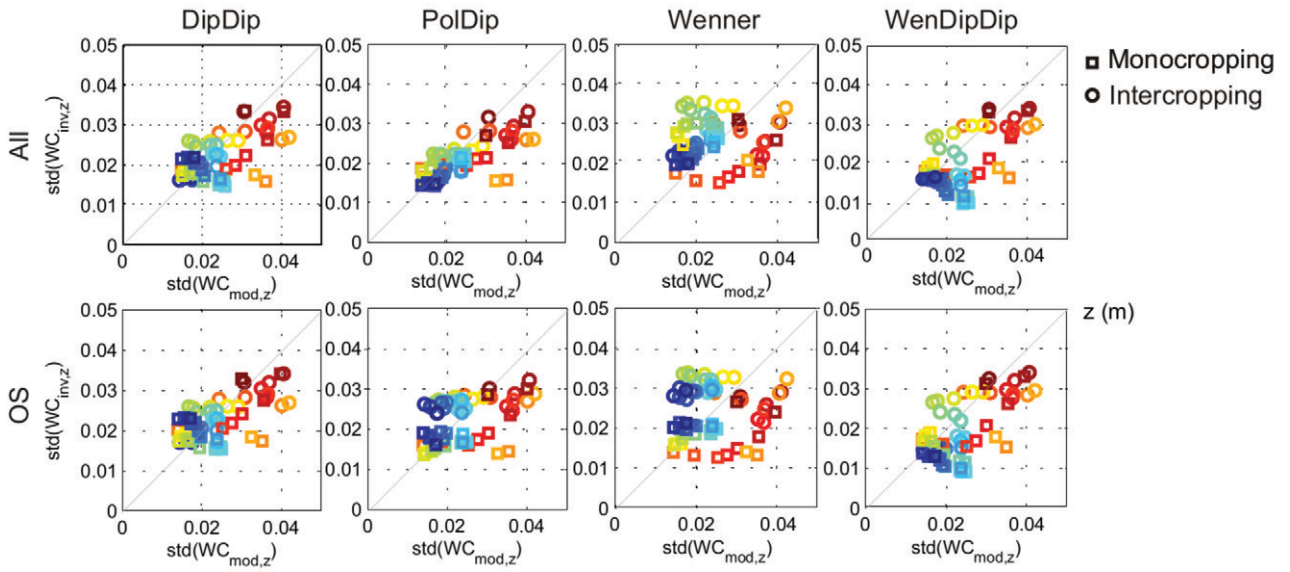

Fig. 8. Standard deviation of the modeled and inverted water content (WC_{mod}, WC_{inv}) for mono- and intercropping case at t = 60 d for all mesh cells (no cutoff at coverage <0.8).

were not correct, this has the greatest impact on the surface variability (not shown).

Table 3 gives an overview of the adjusted coefficient of determination (R_{adj}^2) for each electrode array under consideration, for each of the three times and for the mono- and the intercropping case. The dipole-dipole array and the combination of Wenner and dipole-dipole measurements give the best result in almost all cases and times. The pure Wenner array is inferior to the others for t = 60 d, but has a similar R_{adj}^2 as the others for the other timesteps. From the table emerges as well that the additional use of deep electrodes often improves the result, but not always. At t = 0 d, the difference between with and without deeper electrodes is marginal. The bad result of PolDip (MC, t = 108 d) results from the emergence of a high resistivity zone in the bottom right part of the soil profile which is not present in the model (see Fig. 5). Note that for the computation of the adjusted R_{adj}^2, only mesh cells with a coverage >0.8 are included.

Table 3 also shows the effect of faulty electrode locations on the inversion result. Since it is often difficult to get accurate electrode positions in the field using a measuring tape, this type of error

Table 3. Adjusted coefficients of determination of the model and inverted water content for all simulated array types and timeframes. Cells with log10(coverage) < 0.8 were excluded from calculation.

		MC†				IC			
		All	All‡	OS	OS‡	All	All‡	OS	OS‡
0 d	DipDip§	0.87		0.86		0.87		*0.86*	
	PolDip	0.79		0.89		0.79		*0.89*	
	Wenner	0.88		0.88		0.88		*0.88*	
	WenDipDip					0.87		*0.86*	
60 d	DipDip	0.64	0.06	0.62	0.12	0.70	0.34	0.71	0.41
	PolDip	0.56	−0.02	0.62	0.05	0.58	0.31	0.72	0.33
	Wenner	0.50	−0.13	0.52	−0.04	0.67	0.23	0.68	0.23
	WenDipDip	0.65	0.06	0.65	0.13	0.76	0.37	0.76	0.44
108 d	DipDip	0.28		0.29		0.59		0.55	
	PolDip	0.03		0.34		0.49		0.46	
	Wenner	0.50		0.51		0.57		0.55	
	WenDipDip	0.20		0.22		0.54		0.52	

† MC, monocropping; IC, intercropping.
‡ Result with electrode misplacement
§ DipDip, dipole-dipole; PolDip, pole-dipole; WenDipDip, combination of Wenner and Dipole-dipole.

might affect a lot of already published experimental data. The gray R_{adj}^2 at t = 60 d indicate the inversions with electrode misplacement. Electrode misplacement reduces the quality of the inversion strongly; for the R_{adj}^2 even lowers with 0.25–0.5 units for all arrays tested. The effect seems to be more distinct for the monocropping than for the intercropping case. This indicates that the effect of electrode misplacement depends on the medium in which the measurements are conducted.

Another way to look at spatial variability is the semivariogram. As we know from the previous measures that the highest spatial variability is present between 0 and −1 m depth, we used only this part of the soil region to compute the semivariogram. Figure 9a and 9b shows the semivariograms of the soil moisture for both the mono- and the intercropping case at t = 60 d using 70 lag distances of 0.1 m. The variograms show us how the spatial variance of the inverted water contents chances with electrode array, which systematic spatial structures are present in the mono- and the intercropping system and how well these structures are retrieved after inversion. In the monocropping case a clear periodicity can be seen in the model semivariogram, caused by the presence of maize plant roots at regular intervals of about 0.75 m. A similar, but more complex pattern represents the intercropping case. As the simulation contains not only maize, but also a Leucaena root zone and pieces of bare soil, the effects of different structures are visible, e.g. the distance between two Leucaena hedges is visible in the semivariogram (6 m). All electrode arrays produce a similar, but smoothened or flattened semivariogram. The sill of the inverted semivariograms, which is the limit of the semivariogram tending to infinity lag distances, is lower than the modeled one. The combination of Wenner and dipole-dipole arrays gives the best result. The Wenner array has the most difficulties to reproduce the spatial structure of both cases, which emerges from the very small amplitude of the periodicity in the semivariogram. The arrays using only surface electrodes behave similar to those with deeper electrodes for the dipole-dipole and combination array. For pole-dipole and Wenner, the use of only surface electrodes has a larger negative effect on the outcome. Overall, the difference between cropping systems is visible for all arrays and the presence of root water uptake bulbs can be detected.

Finally, the effect of different pedo-physical relationships on the spatial distribution of inverted soil moisture is shown in Fig. 9c and 9d. The different pedo-physical functions result in a different spatial variability in resistivity. However, when converting inverted resistivities back to WC, the result of all four pedo-physical functions is similar. The slight differences reflect the impact of the smoothing in the ERT inversion leading to slightly different sills of the retrieved water content distributions. However, it can be stated that the use of a 'faulty' pedophysical function which lies within values of literature data, does not affect the inversion quality to a large extent. This means that for modeling purposes looking at spatial patterns, one can use literature data to optimize the measurement array for experimental work. However, it is clear that this should not be done to obtain soil moisture data from ERT

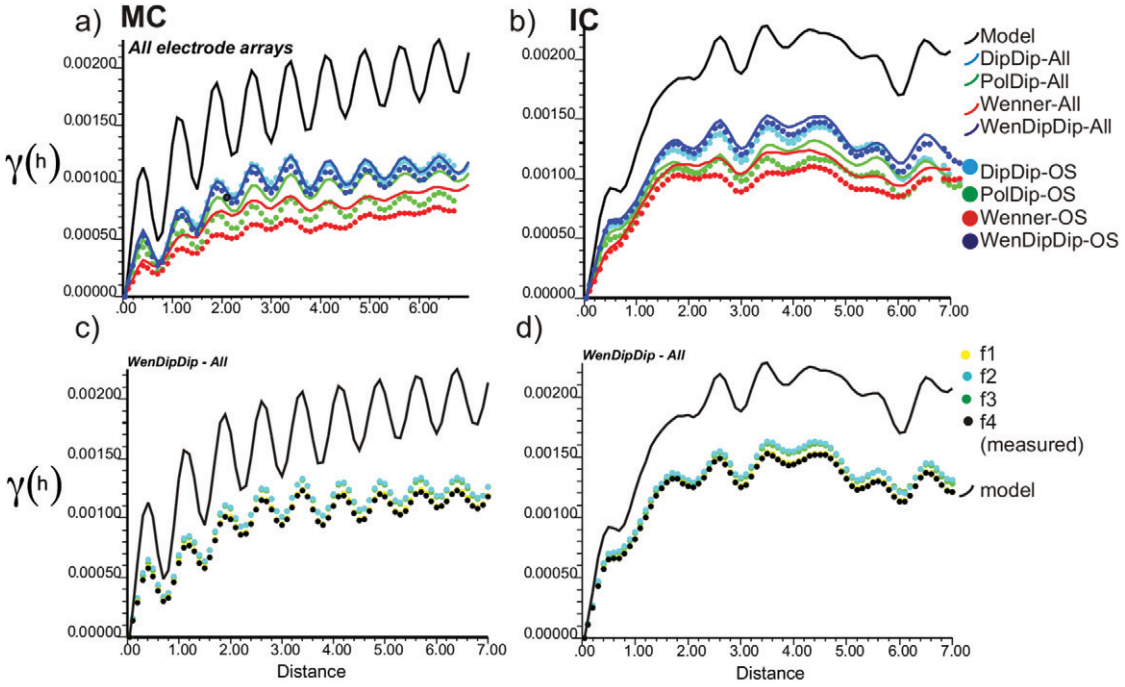

Fig. 9. Semivariograms of the water content (WC) of the synthetic and the inverted WC at Day 60 for the (a) monocropping (MC) and (b) intercropping (IC) case. (c) and (d) give model, the inversion for array WenDipDip-All and the inversion for WenDipDip-OS for all four pedo-physical functions for the monocropping and the intercropping case, respectively.

data in a real experiment when it is important to also estimate the absolute values of soil moisture content.

Resolution

The resolution radius for all array types and for $t = 60$ and $t = 108$ d of the monocropping system is given in Fig. 10. The results for the intercropping system are not shown here, but are very similar. For the pure dipole-dipole and the combination of Wenner & Dipole-dipole, the resolution radius remains under a maximum of 2 m for all cells and for most cells it is smaller than 0.25 m. The pole-dipole and the Wenner array exhibit a strong increase of the resolution radius for the deeper mesh cells. This increase is more markedly for $t = 60$ d than at $t = 108$ d. This is especially the case for the Wenner array. The insertion of deeper electrodes gives very small areas around the electrode location with decreased resolution radius. However, the effect is limited. The largest effect of removing the deeper electrodes on the resolution radius appears in the pole-dipole array. When comparing the distribution of $t = 60$ and $t = 108$ d, an effect on r emerges caused by the different resistivity distribution in the timeframes. In the last timeframe, a strong vertical contrast in resistivity causes the pattern of the resolution radius to flatten at the bottom. This effect is most visible for the Wenner array.

Discussion and Conclusions

The general course of the one-dimensional WC profiles was well reproduced by the different ERT measurement. The largest deviations occurred where sharp jumps in water content occurred (boundary between two soil horizons, infiltration fronts, etc.). The resulting contrasts pose an extra difficulty for smoothness-constrained inversion of the resistivity data. All electrode arrays produce similar results in terms of one-dimensional profiles. Below −2 m, the arrays without deeper electrodes performed worse than the ones with additional electrodes at −0.25 m and −0.50 m.

The standard deviations of water contents at a certain depth and the semivariograms showed that the extent of the spatial variability is generally underestimated and smoothened by the ERT inversion, but the spatial structures remain present in the retrieved WC distributions. The main reason for the underestimation is probably the smoothness-constrained inversion, causing strong contrasts to fade out after inversion. This was already seen in studies using ERT to measure solute transport in soils (e.g., Vanderborght et al., 2005).

The spatial variability is best reproduced by an array combining Wenner and dipole-dipole quadrupoles, probably since it combines the resolving power for horizontal structures of the Wenner array with the resolving power for vertical structures of the dipole-dipole array. The pole-dipole and Wenner arrays generally gave worse results than the other arrays. From the semivariograms, it was clear that not including deeper electrodes deteriorated the result most for these arrays. Using only surface electrodes was generally not beneficial for the inversion result, but the effect was less important for the other arrays. This limited effect was also clear from the mainly local impact on the resolution radius.

The standard deviations and consequently the sill of the semivariogram were underestimated more strongly by the Wenner and the pole-dipole array than by the others. Looking at the resolution radius, the Wenner and pole-dipole array showed a stronger increase of resolution radius with depth than the others, explaining the underestimation of the variability. These results show that it is important to estimate the spatially varying resolution for a measurement array

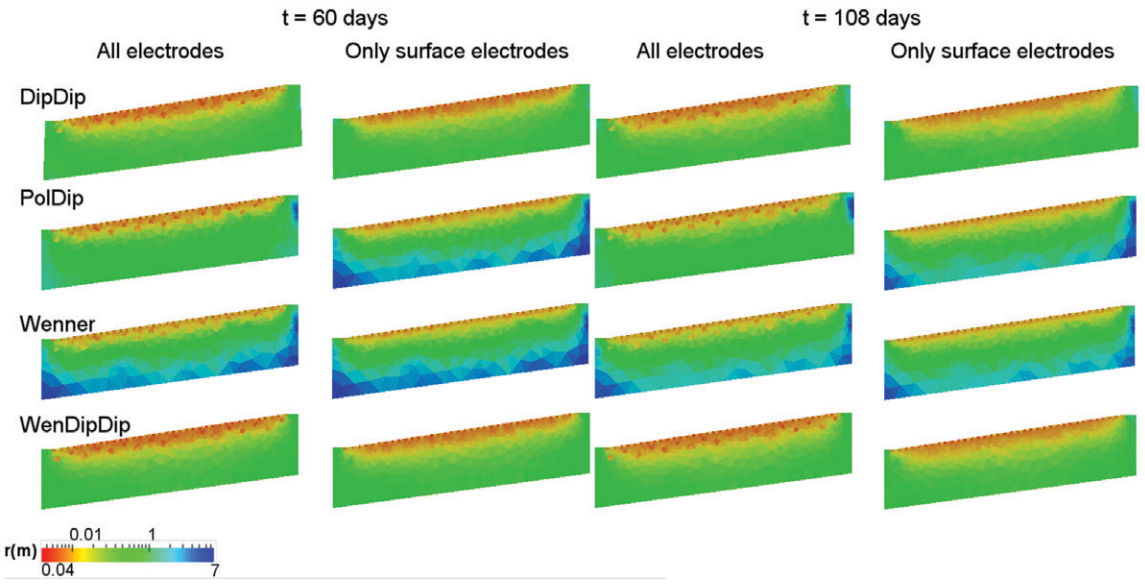

Fig. 10. Distribution of the resolution radius (r) for all arrays at $t = 60$ and 108 d for the monocropping case.

to be sure to capture the phenomena under consideration as precise as possible. However, this need of estimating the spatial distribution beforehand can be avoided by calculating and using the complete data set as presented by Blome et al. (2011).

The choice of a pedo-physical function affects the range of the resistivity values obtained for forward modeling, but also slightly the spatial patterns of resistivity. Changes in the resistivity range are not problematic for the approach presented in this study, since we are mainly interested in patterns of soil moisture and how they change in time. Changes in the spatial patterns could be problematic, however, since the inversion performance can be different in different media. In our case, we could see that the location of spatial structures remained the same for all four functions, which were chosen from literature and fit to measurements in the field, and also the magnitude of the variability was very similar. The effect of using 'faulty' pedo-physical functions within the borders of literature data on inversion errors is therefore only very small and can be neglected for simulation issues if the main interest is to reproduce spatial structures and not to find correct absolute range of resistivities.

The effect of electrode misplacement was mainly visible at the surface of the profile and had a strong negative effect on the adjusted coefficient of determination. Electrode misplacement causes resistivity artifacts in the neighborhood of the electrodes, which is per definition on and near the surface. The artifacts compensate for faulty geometric factors and cause a bad model recovery. Especially for field experiments, it is important to measure the electrode location as exact as possible to avoid this kind of error. If the misfit is systematic (as in this case); it can be avoided using an appropriate timelapse inversion scheme (LaBrecque et al., 1996).

ERT can be used to observe effects of cropping systems on soil moisture distribution. Using on-site calibration of pedo-physical parameters, the measurements reproduce the range of water contents well. A major disadvantage of the classical smoothness-constrained inversion is the fact that sharp resistivity transitions are not well reproduced. If additional information on the thickness of soil horizons is available, they should be included in a starting or reference model and contrast should be allowed at the known boundaries. ERT can handle different types of spatial variability potentially present in mono- and intercropping systems at different stages of the growing season. The virtual measurements showed that it is possible to retrieve differences between two cropping systems on the same soil and under the same climatic conditions. Note that the selected timeframes were chosen for their representativeness for different stages in the growing season and because they represent 'extremes': from no effect of crops visible over distinct root water uptake bulbs under dry conditions and infiltration during prolonged rainfall events at the end of the growing season. Under wetter conditions, it might be difficult to distinguish single root water uptake regions below the rows by observing the spatial distribution of the data. This would be caused by a quick redistribution of soil moisture in the profile and low resistivities everywhere in the profile. Here, the use of a semivariogram might be the line to take, since it will reveal spatial structures which are not always clearly visible by the bare eye.

Acknowledgments

We thank the KULeuven Research fund for financing this work within the framework of the project OT/07/045.

References

Aaltonen, J., and B. Olofsson. 2002. Direct current (DC) resistivity measurements in long-term groundwater monitoring programmes. Environ. Geol. (Berl.) 41:662–671.

Agus, F., D.K. Cassel, and D.P. Garrity. 1997. Soil-water and soil physical properties under contour hedgerow systems on sloping oxisols. Soil Tillage Res. 40:185–199. doi:10.1016/S0167-1987(96)01069-0

al Hagrey, S.A. 2007. Geophysical imaging of root-zone, trunk, and moisture heterogeneity. J. Exp. Bot. 58:839–854. doi:10.1093/jxb/erl237

al Hagrey, S.A., and T. Petersen. 2011. Numerical and experimental mapping of small root zones using optimized surface and borehole resistivity tomography. Geophysics 76:G25–G35.

Allen, R.G., L.S. Pereira, D. Raes, and M. Smith. 1998. Crop evapotranspiration—Guidelines for computing crop water requirements. R.G. Allen, editor. FAO, Rome.

Alumbaugh, D.L., and G.A. Newman. 2000. Image appraisal for 2-D and 3-D electromagnetic inversion. Geophysics 65:1455–1467.

Amato, M., B. Basso, G. Celano, G. Bitella, G. Morelli, and R. Rossi. 2008. In situ detection of tree root distribution and biomass by multi-electrode resistivity imaging. Tree Physiol. 28:1441–1448.

Amato, M., G. Bitella, R. Rossi, J.A. Gómez, S. Lovelli, and J.J.F. Gomes. 2009. Multi-electrode 3D resistivity imaging of alfalfa root zone. Eur. J. Agron. 31:213–222. doi:10.1016/j.eja.2009.08.005

Amidu, S.A., and J.A. Dunbar. 2007. Geoelectric studies of seasonal wetting and drying of a Texas vertisol. Vadose Zone J. 6:511–523. doi:10.2136/vzj2007.0005

Archie, G.E. 1942. The electrical resistivity log as an aid in determining some reservoir characteristics. Trans. Am. Inst. Min. Metall. Pet. Eng. 146:54–67.

Besson, A., I. Cousin, A. Samouëlian, H. Boizard, and G. Richard. 2004. Structural heterogeneity of the soil tilled layer as characterized by 2D electrical resistivity surveying. Soil Tillage Res. 79:239–249. doi:10.1016/j.still.2004.07.012

Blome, M., H. Maurer, and S. Greenhalgh. 2011. Geoelectric experimental design–Efficient acquisition and exploitation of complete pole-bipole data sets. Geophysics 76:F15–F26.

Carsel, R.F. and R.S. Parrish. 1988. Developing joint probability distributions of soil water retention characteristics. Water Resour. Res. 24: 755–769. doi:10.1029/WR024i005p00755

Celano, G., A.M. Palese, A. Ciucci, E. Martorella, N. Vignozzi, and C. Xiloyannis. 2011. Evaluation of soil water content in tilled and cover-cropped olive orchards by the geoelectrical technique. Geoderma Corrected Proof. (in press).

Celano, G., A.M. Palese, A.C. Tuzio, D. Zuardi, L. Lazzari, C. Xilloyanis, and E. Martorella. 2010. Geo-electrical survey on the soil of an apricot orchard grown under semi-arid conditions. In: C. Xiloyannis, editor, XIVth IS on apricot breeding and culture. International Society for Horticultural Science, Leuven, Belgium.

Cousin, I., A. Besson, H. Bourennane, C. Pasquier, B. Nicoullaud, D. King, and G. Richard. 2009. From spatial-continuous electrical resistivity measurements to the soil hydraulic functioning at the field scale. C. R. Geosci. 341:859–867. doi:10.1016/j.crte.2009.07.011

Craswell, E.T., A. Sajjapongse, D.J.B. Howlett, and A.J. Dowling.1997. Agroforestry in the management of sloping lands in Asia and the Pacific. Agrofor. Syst. 38:121–137. doi:10.1023/A:1005960612386

Curtis, A. 1999. Optimal experiment design: Cross-borehole tomographic examples. Geophys. J. Int. 136:637–650. doi:10.1046/j.1365-246x.1999.00749.x

Danielsen, B.E., and T. Dahlin. 2010. Numerical modelling of resolution and sensitivity of ERT in horizontal boreholes. J. Appl. Geophys. 70:245–254. doi:10.1016/j.jappgeo.2010.01.005

Dercon, G., J. Deckers, J. Poesen, G. Govers, H. Sánchez, M. Ramírez, R. Vanegas, E. Tacuri, and G. Loaiza. 2006. Spatial variability in crop response under contour hedgerow systems in the Andes region of Ecuador. Soil Tillage Res. 86:15–26. doi:10.1016/j.still.2005.01.017

Deutsch, C.V., and A.G. Journel. 1997. GSLIB: Geostatistical software library and user's guide. 2nd ed. Applied geostatistics series. Oxford Univ. Press, Oxford.

Dey, A., and H.F. Morrison. 1979. Resistivity modelling for arbitrarily shaped two-dimensional structures. Geophys. Prospect. 27:106–136. doi:10.1111/j.1365-2478.1979.tb00961.x

Essig, E.T., C. Corradini, R. Morbidelli, and R.S. Govindaraju. 2009. Infiltration and deep flow over sloping surfaces: Comparison of numerical and experimental results. J. Hydrol. 374:30–42. doi:10.1016/j.jhydrol.2009.05.017

Feddes, R.A., P. Kowalik, and H. Zaradny. 1978. Simulation of field water use and crop yield. Simulation monographs. PUDOC, Wageningen, the Netherlands.

Friedel, S. 2003. Resolution, stability and efficiency of resistivity tomography estimated from a generalized inverse approach. Geophys. J. Int. 153:305–316. doi:10.1046/j.1365-246X.2003.01890.x

Furman, A., T.P.A. Ferre, and A.W. Warrick. 2003. A sensitivity analysis of electrical resistivity tomography array types using analytical element modeling. Vadose Zone J. 2:416–423.

Garré, S., M. Javaux, J. Vanderborght, L. Pages, and H. Vereecken. 2011. Three-dimensional electrical resistivity tomography to monitor root zone water dynamics. Vadose Zone J. 10:412–424. doi:10.2136/vzj2010.0079

Günther, T. 2004. Inversion methods and resolution analysis for the 2D/3D reconstruction of resistivity structures from DC Measurements. Ph.D. diss. Univ. of Mining and Technol., Freiberg, Germany.

Günther, T., C. Rücker, and K. Spitzer. 2006. Three-dimensional modelling and inversion of DC resistivity data incorporating topography- II. Inversion. Geophys. J. Int. 166:506–517. doi:10.1111/j.1365-246X.2006.03011.x

Gutiérrez-Jurado, H.A., E.R. Vivoni, J.B.J. Harrison, and H. Guan. 2006. Ecohydrology of root zone water fluxes and soil development in complex semiarid rangelands. Hydrol. Processes 20:3289–3316. doi:10.1002/hyp.6333

Hairiah, K., M. Van Noordwijk, and G. Cadisch. 2000. Crop yield, C and N balance of three types of cropping systems on an Ultisol in Northern Lampung. NJAS- Wageningen. J. Life Sci. 48:3–17.

Harr, R.D. 1977. Water flux in soil and subsoil on a steep forested slope. J. Hydrol. 33:37–58. doi:10.1016/0022-1694(77)90097-X

Hornberger, G.M., P.F. Germann, and K.J. Beven. 1991. Throughflow and solute transport in an isolated sloping soil block in a forested catchment. J. Hydrol. 124:81–99. doi:10.1016/0022-1694(91)90007-5

Imo, M., and V.R. Timmer. 2000. Vector competition analysis of a Leucaena-maize alley cropping system in western Kenya. For. Ecol. Manage. 126:255–268. doi:10.1016/S0378-1127(99)00091-2

Jayawickreme, D.H., R.L. Van Dam, and D.W. Hyndman. 2010. Hydrological consequences of land-cover change: Quantifying the influence of plants on soil moisture with time-lapse electrical resistivity. Geophysics 75:WA43–WA50.

Kemna, A., J. Vanderborght, B. Kulessa, and H. Vereecken. 2002. Imaging and characterisation of subsurface solute transport using electrical resistivity tomography (ERT) and equivalent transport models. J. Hydrol. 267:125–146. doi:10.1016/S0022-1694(02)00145-2

Koestel, J., J. Vanderborght, M. Javaux, A. Kemna, A. Binley, and H. Vereecken. 2009. Non-invasive 3D transport characterization in a sandy soil using ERT I: Investigating the validity of ERT-derived transport parameters. Vadose Zone J. 8:711–722. doi:10.2136/vzj2008.0027

LaBrecque, D.J., M. Miletto, W. Daily, A. Ramirez, and E. Owen. 1996. The effects of noise on Occam's inversion of resistivity tomography data. Geophysics 61:538–548.

Lal, R. 1989. Agroforestry systems and soil surface management of a tropical alfisol. Agrofor. Syst. 8:97–111. doi:10.1007/BF00123115

Lal[illegible] C. Roisin, M. Javaux, M. Vanclooster, and C.L. Bielders. 2011. Electrical resistivity in a structured agricultural loamy soil: Identification of the appropriate pedo-physical model and field application. Water Resour. Res.10:1023–1033.

Linde, N., A. Binley, A. Tryggvason, L.B. Pedersen, and A. Revil. 2006. Improved hydrogeophysical characterization using joint inversion of cross-hole electrical resistance and ground-penetrating radar traveltime data. Water Resour. Res. 42(12):W04410.

Loke, M.H., and R.D. Barker. 1996. Practical techniques for 3D resistivity surveys and data inversion. Geophys. Prospect. 44:499–523. doi:10.1111/j.1365-2478.1996.tb00162.x

Maurer, H., D.E. Boerner, and A. Curtis. 2001. Design strategies for electromagnetic geophysical surveys. Inverse Probl. 17:189. doi:10.1088/0266-5611/17/1/501

Menke, W. 1989. Geophysical data analysis: Discrete inverse theory. Academic Press, New York.

Michot, D., Y. Benderitter, A. Dorigny, B. Nicoullaud, D. King, and A. Tabbagh. 2003. Spatial and temporal monitoring of soil water content with an irrigated corn crop cover using surface electrical resistivity tomography. Water Resour. Res. 39: 1138–1158.

Michot, D., A. Dorigny, and Y. Benderitter. 2001. Determination of water flow direction and corn roots-induced drying in an irrigated Beauce CALCISOL, using electrical resistivity measurements. Comptes Rendus De L Academie Des Sciences Serie Ii Fascicule a-Sciences De La Terre Et Des Planetes 332:29–36.

Morgan, R.P.C. 2004. Soil Erosion and Conservation. Wiley-Blackwell, New York.

Müller, K., J. Vanderborght, A. Englert, A. Kemna, J.A. Huisman, J. Rings, and H. Vereecken. 2010. Imaging and characterization of solute transport during two tracer tests in a shallow aquifer using electrical resistivity tomography and multilevel groundwater samplers. Water Resour. Res. 46:W03502. doi:10.1029/2008WR007595

Mushagalusa, G.N., J.-F. Ledent, and X. Draye. 2008. Shoot and root competition in potato/maize intercropping: Effects on growth and yield. Environ. Exp. Bot. 64:180–188. doi:10.1016/j.envexpbot.2008.05.008

Nijland, W., M. van der Meijde, E.A. Addink, and S.M. de Jong. 2010. Detection of soil moisture and vegetation water abstraction in a Mediterranean natural area using electrical resistivity tomography. Catena 81:209–216. doi:10.1016/j.catena.2010.03.005

Noel, M., and B. Xu. 1991. Archeological investigation by electrical resistivity tomography: A preliminary study. Geophys. J. Int. 107:95–102. doi:10.1111/j.1365-246X.1991.tb01159.x

Oldenborger, G.A., and P.S. Routh. 2009. The point-spread function measure of resolution for the 3-D electrical resistivity experiment. Geophys. J. Int. 176:405–414. doi:10.1111/j.1365-246X.2008.04003.x

Pansak, W., G. Dercon, T. Hilger, T. Kongkaew, and G. Cadisch. 2007. 13C isotopic discrimination: A starting point for new insights in competition for nitrogen and water under contour hedgerow systems in tropical mountainous regions. Plant Soil 298:175–189. doi:10.1007/s11104-007-9353-y

Raes, D., P. Steduto, T.C. Hsiao, and E. Fereres. 2009. Aquacrop-the FAO Crop Model to Simulate Yield Response to Water: Ii. Main Algorithms and Software Description. Agron. J. 101:438–447. doi:10.2134/agronj2008.0140s

Revil, A., and P.W.J. Glover. 1998. Nature of surface electrical conductivity in natural sands, sandstones, and clays. Geophys. Res. Lett. 25:691–694. doi:10.1029/98GL00296

Rossi, R., M. Amato, G. Bitella, R. Bochicchio, J.J. Ferreira Gomes, S. Lovelli, E. Martorella, and P. Favale. 2011. Electrical resistivity tomography as a non-destructive method for mapping root biomass in an orchard. Eur. J. Soil Sci. 62:206–215. doi:10.1111/j.1365-2389.2010.01329.x

Rücker, C., T. Günther, and K. Spitzer. 2006. Three-dimensional modelling and inversion of dc resistivity data incorporating topography- I. Modelling. Geophys. J. Int. 166:495–505. doi:10.1111/j.1365-246X.2006.03010.x

Šimůnek, J., M. Šejna, and M.T. van Genuchten. 1996. The Hydrus-2D software package for simulating water flow and solute transport in two-dimensional variably saturated media. Version 1.0. IGWMC- TPS- 53. International Ground Water Modeling Center, Colorado School of Mines, Golden, CO.

Singha, K., and S.M. Gorelick. 2005. Saline tracer visualized with three-dimensional electrical resistivity tomography: Field-scale spatial moment analysis. Water Resour. Res. 41:W05023.

Spies, B.R. 1989. Depth of investigation in electromagnetic sounding methods. Geophysics 54:872–888.

Srayeddin, I., and C. Doussan. 2009. Estimation of the spatial variability of root water uptake of maize and sorghum at the field scale by electrical resistivity tomography. Plant Soil 319:185–207. doi:10.1007/s11104-008-9860-5

Steduto, P., T.C. Hsiao, D. Raes, and E. Fereres. 2009. AquaCrop-The FAO crop model to simulate yield response to water: I. Concepts and Underlying Principles. Agron. J. 101:426–437.

Stummer, P., H. Maurer, and A.G. Green. 2004. Experimental design: Electrical resistivity data sets that provide optimum subsurface information. Geophysics 69:120–139.

Tang, Y. 2000. Manual on contour hedgerow intercropping technology. ICIMOD, Katmandu, Nepal.

Theil, H. 1971. Principles of econometrics. John Wiley and Sons, New York.

Turkelboom, F., J. Poesen, I. Ohler, K. Van Keer, S. Ongprasert, and K. Vlassak. 1997. Assessment of tillage erosion rates on steep slopes in northern Thailand. Catena 29:29–44. doi:10.1016/S0341-8162(96)00063-X

van Genuchten, M.Th. 1980. A closed form equation for predicting the hydraulic conductivity of unsaturated soils. Soil Sci. Soc. Am. J. 44:892–898. doi:10.2136/sssaj1980.03615995004400050002x

Vanderborght, J., A. Kemna, H. Hardelauf, and H. Vereecken. 2005. Potential of electrical resistivity tomography to infer aquifer transport characteristics from tracer studies: A synthetic case study. Water Resour. Res.41: W06013.

Waxman, M.H., and L.J.M. Smits. 1968. Electrical conductivities in oil-bearing shaly sands. Soc. Pet. Eng. J. 8:107.

Werban, U., S.A. al Hagrey, and W. Rabbel. 2008. Monitoring of root-zone water content in the laboratory by 2D geoelectrical tomography. J. Plant Nutr. Soil Sci. 171:927–935.

Wilkinson, P.B., J.E. Chambers, M. Lelliott, G.P. Wealthall, and R.D. Ogilvy. 2008. Extreme sensitivity of crosshole electrical resistivity tomography measurements to geometric errors. Geophys. J. Int. 173:49–62. doi:10.1111/j.1365-246X.2008.03725.x

Xu, B.W., and M. Noel. 1993. On the Completeness of Data Sets with Multielectrode systems for electrical-resistivity survey. Geophys. Prospect. 41:791–801. doi:10.1111/j.1365-2478.1993.tb00885.x

Zenone, T., G. Morelli, M. Teobaldelli, F. Fischanger, M. Matteucci, M. Sordini, A. Armani, C. Ferre, T. Chiti, and G. Seufert. 2008. Preliminary use of ground-penetrating radar and electrical resistivity tomography to study tree roots in pine forests and poplar plantations. Commonwealth Scientific and Industrial Research Organization, Collingwood, Australia.